Microsc. Microanal. 18, 1220–1228, 2012
doi:10.1017/S1431927612013414

Microscopy AND Microanalysis

Three-Dimensional Electron Energy Deposition Modeling of Cathodoluminescence Emission near Threading Dislocations in GaN and Electron-Beam Lithography Exposure Parameters for a PMMA Resist

Hendrix Demers,[1] Nicolas Poirier-Demers,[1] Matthew R. Phillips,[2] Niels de Jonge,[3,†] and Dominique Drouin[1,*]

[1]*Universite de Sherbrooke, Electrical and Computer Engineering Department, Sherbrooke, Quebec J1K 2R1, Canada*
[2]*University of Technology, Microstructural Analysis Unit, Faculty of Science, Sydney, NSW 2007, Australia*
[3]*Vanderbilt University School of Medicine, Department of Molecular Physiology and Biophysics, Nashville, TN 37232-0615, USA*

Abstract: The Monte Carlo software CASINO has been expanded with new modules for the simulation of complex beam scanning patterns, for the simulation of cathodoluminescence (CL), and for the calculation of electron energy deposition in subregions of a three-dimensional (3D) volume. Two examples are presented of the application of these new capabilities of CASINO. First, the CL emission near threading dislocations in gallium nitride (GaN) was modeled. The CL emission simulation of threading dislocations in GaN demonstrated that a better signal-to-noise ratio was obtained with lower incident electron energy than with higher energy. Second, the capability to simulate the distribution of the deposited energy in 3D was used to determine exposure parameters for polymethylmethacrylate resist using electron-beam lithography (EBL). The energy deposition dose in the resist was compared for two different multibeam EBL schemes by changing the incident electron energy.

Key words: cathodoluminescence (CL), electron-beam lithography, energy deposition, Monte Carlo simulations, resist, threading dislocation, three-dimensional (3D)

Introduction

In a scanning electron microscope (SEM), the sample is modified by the incident electrons via a number of energy-loss mechanisms, where part or the entire primary energy is deposited within the sample. This alteration can either be temporary (a dynamic system) or permanent (a static system). For temporary modification, we assume in this work that the sample returns to its original state after electron-beam irradiation. Cathodoluminescence (CL) generation from a material with short carrier lifetime or where the SEM scan rate is slower than the excitation relaxation time are examples of temporary modification. Here, electron-energy loss occurs by promoting electrons from the valence band into the conduction band, which emits light when they relax. The CL signal is proportional to the amount of deposited energy in a region of the sample for each scan point (Toth & Phillips, 1998). Conversely electron-beam lithography (EBL) is an example of permanent modification of the sample, where the incident electrons irreversibly break the bonds or crosslink molecules of the resist and the exposure depends on the total deposited energy by all scan points. The relationship between the energy deposition and these two techniques can be modeled using the Monte Carlo (MC) simulation method.

Two-dimensional (2D) CL modeling of thin films (Fleischer et al., 1999; Gelhausen et al., 2001) and vertical multilayer (Toth & Phillips, 1998; Toth, 2006) was simulated with a previous version of the MC software CASINO (Hovington et al., 1997*a*). Similar CL modeling applications were obtained with different MC software (Holt & Napchan, 1994; Barjon et al., 2003). However, the simulation of CL emission in a sample with nonradiative recombination area, such as dislocation, was not possible with these MC software. A MC model was proposed to included a nonradiative recombination area (Nouiri & Aouati, 2008), but did not include the effect of the diffusion length in the simulation.

The MC method was also used to study the influence of electron scattering on the resolution of EBL (Greeneich & Duzer, 1974; Kyser & Viswanathan, 1975; Adesida et al., 1979; Murata et al., 1981, 1987; Glezos et al., 1992; Raptis et al., 1993; Glezos & Raptis, 1996; Kim et al., 1998). The EBL simulation consists of three major steps: the electron-beam exposure, the fragmentation of the resist molecule, and the development of the exposed EBL resist. The electron-beam exposure was studied with the MC method in a complete simulation of the EBL process (Aktary et al., 2006; Babin et al., 2006; Zhou & Yang, 2006; Stepanova et al., 2010). Thus far, none of the software combined the following three features: (1) the simulation of three-dimensional

Received March 15, 2012; accepted September 9, 2012
*Corresponding author. E-mail: Dominique.Drouin@USherbrooke.ca
†Current address: INM Leibniz-Institute for New Materials, Campus D2 2, 66123 Saarbrücken, Germany

(3D) sample, (2) complex beam scanning (scan point) patterns, and (3) the 3D representation of the deposited energy.

Here, we present the latest version of the MC software CASINO Version 3, which includes new features to model the signal generated by the deposited energy in the sample. These features allow the simulation of nonradiative recombination area, including the effect of the diffusion length and the simulation of the 3D electron-resist interaction effect on the electron-beam exposure for any electron-beam exposure patterns and for a 3D specimen. The new features in the software are (1) the simulation of complex beam scanning (scan point) patterns, (2) the simulation of CL, and (3) the calculation of electron energy deposition in subregions of a 3D specimen. In this article two examples are presented on the application of the new energy deposition modeling capabilities of CASINO. First, CL emission near threading dislocations in gallium nitride (GaN) is modeled. Second, the use of this modeling approaches to determine exposure parameters using EBL in polymethylmethacrylate (PMMA) resist.

Methods

The energy deposited by incident electrons was simulated with the CASINO Version 3 Monte Carlo software, which includes the simulation of 3D samples (Demers et al., 2011). The software can be downloaded at www.gel.usherbrooke.ca/casino/index.html and used freely. The Monte Carlo calculations approach used in CASINO Version 3 was based on previous version of CASINO (Drouin et al., 1997, 2007; Hovington et al., 1997*a*, 1997*b*) and previous work of others (Bishop, 1965; Gauvin & L'Espérance, 1992; Joy, 1995).

In CASINO, each electron trajectory is simulated by computing the elastic scattering events. The inelastic events are approximated by the mean energy loss between two elastic scattering events. The calculation of each electron trajectory is done as follows. The initial position and energy of the electron are calculated from the SEM electron-beam parameters specified by the user. From the initial position, where the electron impinges the sample, the distance D between two successive collisions is evaluated from the electron elastic cross sections (Kyser & Viswanathan, 1975) and a random number (Reimer, 1998). The elastic scattering angle θ is determined from another random number, and the differential elastic cross section is calculated either by using analytical models (Reimer, 1998) or from tabulated values of the inverse relation (Newbury & Myklebust, 1981; Drouin et al., 1997). The energy loss ΔE between two successive collisions is then calculated from the mean energy loss rate dE/dx multiplied by the distance traveled D:

$$\Delta E = \frac{dE}{dx} \cdot D. \tag{1}$$

The mean energy loss rate is given by the modified Bethe equation (Joy & Luo, 1989). This mean energy loss rate depends on the electron energy and the composition of the sample. The trajectory calculation is completed when either the electron exits the sample or the energy of the primary electron falls below a threshold value (50 eV). This threshold energy value can be adjusted in CASINO. However, we did not validate the all physical models for value lower than 50 eV (Demers et al., 2011).

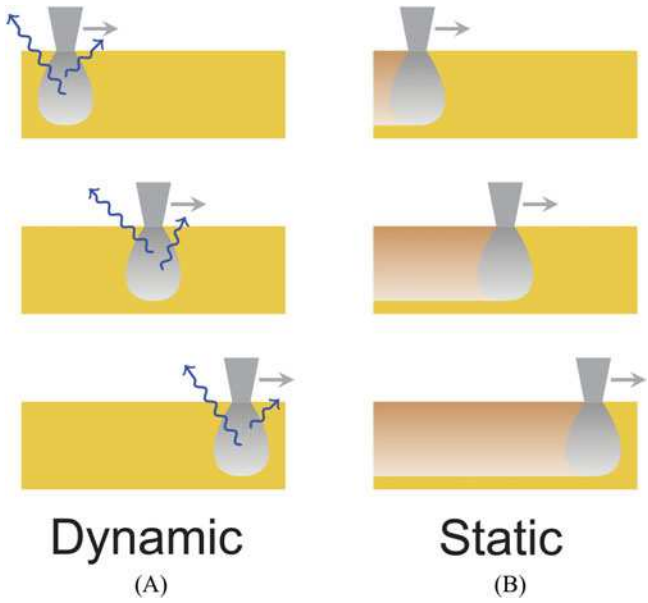

Figure 1. Schematic of two categories of energy deposition by electrons into the sample relative to the beam scan speed: a dynamic system and a static system. **A:** In the dynamic system, the CL emission (blue wave-line) occurred only at the current beam position. **B:** In a static system, sample damage (brown area) was observed even after the beam left the area.

The CASINO software can simulate one or more scan points to form a line scan (one-dimensional) or image (2D). Furthermore, the 2D scan point feature is not limited to a rectangular area. Complex beam scanning patterns are created by importing, from one or more text files, the coordinate of each scan point used in the simulation. The energy deposition by electrons into the sample relative to the beam scan speed can be separated in two categories: a dynamic system and a static system. These two systems are illustrated in Figure 1.

Dynamic System

For a dynamic system, the processes resulting from the deposited energy are temporary with the sample returning to its original state following exposure to the electron beam before moving to the next scan point (Fig. 1A). To simulate such a dynamic system, CASINO calculates the total deposited energy for each region in the sample for each scan point. The calculated signal generated from the deposited energy is the sum in the selected region of the total energy deposited by all electron trajectories for a given scan point. If the interaction volume is large compared to the beam diameter, energy deposition and signal production are possible in regions far away from the scan point position.

Static System

In a static system, the deposited energy results in a permanent change in the sample, or the excitation relaxation time is longer than the total acquisition time of the scan (Fig. 1B). We simulate this system by calculating a deposited energy distribution in 3D volume (Cartesian, cylindrical, or spherical). For all scan points, the total deposited energy 3D distribution was calculated. The 3D volume position is absolute, i.e., a fixed position for all scan points. For each unit volume, the total energy loss for all trajectories and all scan points is summed. To calculate the energy loss inside a unit volume, the mean energy loss rate of the trajectory segment in the unit volume is multiplied by the trajectory length in the volume.

For a dynamic system, the software displays the total deposited energy for the selected region for each scan point as a line scan or image. For a static system, the software displays either a top-down view of the surface (XY) or a cross-sectional view (XZ) of the deposited energy within the sample. These energy distributions are useful to investigate the effect of electron dose and scan properties in SEM and have application in techniques such as EBL, CL, and electron-beam induced current, for example.

Results and Discussion

The following two examples illustrate the application of deposited energy by incident electrons simulated with CASINO in, first, CL microscopy and, second, EBL.

Modeling Threading Dislocation CL Contrast in Gallium Nitride

The CL technique can be used as a method to characterize GaN materials (Pauc et al., 2006). These materials have drawn considerable attention due to their remarkable optical properties and their application as ultraviolet photon emitters, such as light emitting diodes and laser diodes. Significant lattice mismatch and differences in thermal expansion coefficients between GaN epilayer and substrate (sapphire or silicon carbide) result in a large strain at the interface. Strain relieving threading dislocations (TDs) perpendicular to the top surface are generated by the stress created by the lattice mismatch. These strain-relieving TDs might significantly degrade the optoelectronic and electronic device's performance. The TDs in GaN behave as nonradiative recombination channels of infinite velocity and zero dimension and act as charge leakage paths in electronic devices (McCarthy et al., 2001). To understand the relationships between defects and the optical properties of GaN epilayers, CL studies of the recombination processes in the vicinity of TDs at the nanometer scale are needed. A detailed investigation of the correlation between incident electron energy and the luminescence charge collection processes around TDs (diffusion length) is thus pertinent and useful to determine the optimal signal condition and spatial resolution.

The Monte Carlo program CASINO has been adapted for CL applications by adding a deposited energy distribution simulation feature and flexibility to model more realistic SEM samples. With these features it is possible to simulate a complete image of a complex sample featuring multiple regions of different chemical compositions or recombination efficiencies. Such images will show the CL intensity according to the amount of deposited energy within the selected regions. Since the CL intensity is proportional to the deposited energy, it is possible, with such a simulation tool, to investigate the electron-beam interaction effect around TDs with a model of the carrier diffusion length.

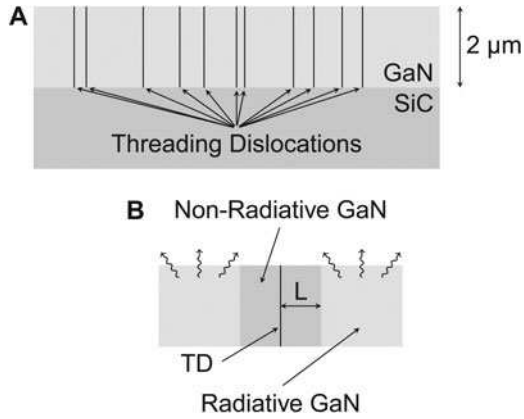

Figure 2. Schematics used for the simulation of the CL near threading dislocation (TD). **A:** Sample geometry (not to scale). Threading dislocations in GaN are perpendicular to the sample top surface. **B:** A vertical cylinder with a radius L of a few ten to hundreds of nanometers was used to model carrier diffusion near the threading dislocation in GaN. The cylinder defined a nonradiative recombination region, and the rest of the GaN film was considered a radiative recombination region.

Figure 2A shows a schematic representation of the GaN sample used in the simulation. The sample was composed of a 2-μm-thick layer of GaN on a SiC substrate. The threading dislocations in a GaN layer were modeled with cylinders of 2 μm in length, perpendicular to the substrate, with the same composition than the GaN layer. The TDs were zero-dimensional vertical lines, but to model carrier diffusion near the TD a GaN vertical cylinder with a radius of a few ten to hundred nanometers was defined as another region in the simulation (Fig. 2B). The cylinder radius was used as a crude model of the carrier diffusion length L to study the relationship between CL generation volume and different values of L. When the carrier was generated at a distance less than the cylinder radius, the nonradiative recombination occurs at the TD. In this study, the carrier diffusion length (cylinder radius) varied from 50 nm to 125 nm; this range represents the variation of the diffusion length with temperature and doping level (Pauc et al., 2006). Because the TDs in GaN behave as nonradiative recombination channels, only the deposited energy in the GaN layer was used as a CL signal. Energy deposited inside the cylinder (TD) did not contribute to the CL emission (see Fig. 2B).

Figure 3 shows several 500 nm $\times$ 500 nm images of the deposited energy in the GaN layer for incident energies

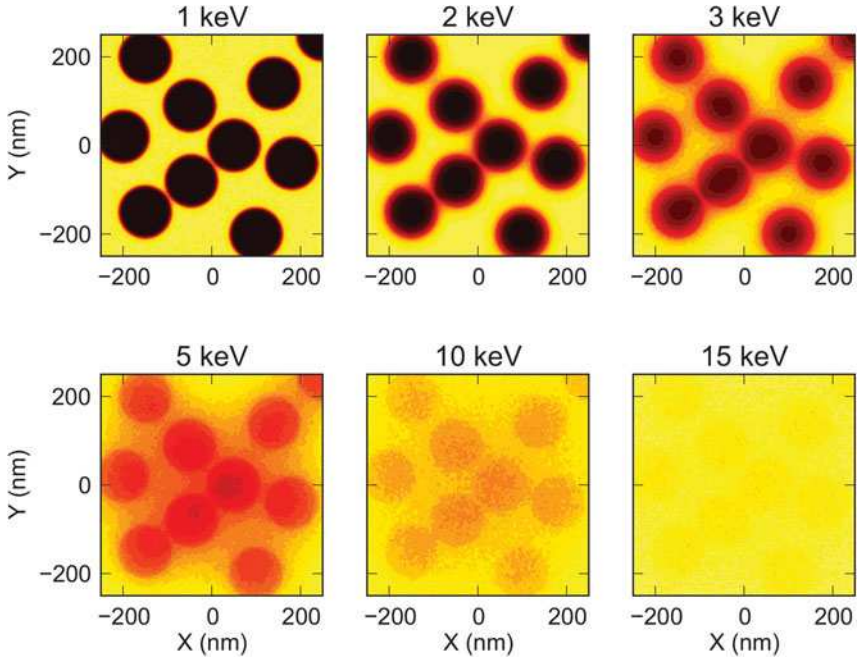

Figure 3. Simulated images of deposited energy per scan point obtained for TDs in GaN with cylinder radius (modeling the diffusion length near TD) of 60 nm. The incident energy E_0 was varied between 1 to 15 keV. The image area was 500 × 500 nm^2. The number of electrons N_0 was changed to keep the nominal deposited energy constant ($E_0 \times N_0$ = 10,000 keV).

between 1 to 15 keV with a scanning step of 1 nm. At each pixel, the intensity corresponds to the total deposited energy in the GaN layer for all the electron trajectories of this scan point. In this work, we suppose that the carrier diffusion and recombination processes are much faster than the scan speed (Joy, 1995), and the system returned to its original state before the next scan point. The nominal number of electrons N_0 is modified for each energy E_0 simulated to keep the nominal deposited energy constant (10,000 keV), which is defined by the product of the E_0 with the electron-beam current I_0 for constant dwell time. For each scan points, the number of electrons is randomly obtained using a Poisson distribution and N_0 to simulate the effect of gun shot noise on the images (Reimer, 1998; de Jonge et al., 2010; Demers et al., 2011).

In Figure 3, strong CL emission is represented by white area and corresponds to dislocation free area. The darker area shows the TD position with the model diffusion range around them. When the energy is increased, the interaction volume increases, which delocalize the CL emission. This effect is observed in Figure 3 by a decrease of contrast between the TDs and the dislocation free GaN areas with larger energy. The CL intensity is proportional to the amount of electron-hole pairs generated in the sample, which scales with deposited energy in the sample.

In GaN, the diffusion length depends on sample temperature and doping level (Pauc et al., 2006). Line scans across a TD were simulated with a scanning step of 1 nm for five energies and two cylinder radii (50 and 100 nm) as shown in Figure 4. The TD is located in the middle of the line scan (at 0 nm). The nominal number of electrons N_0 is again modified for each energy E_0 simulated to keep the nominal deposited energy constant (10,000 keV). The deposited energy in dislocation free GaN area was lower than the nominal deposited energy due to the energy lost from

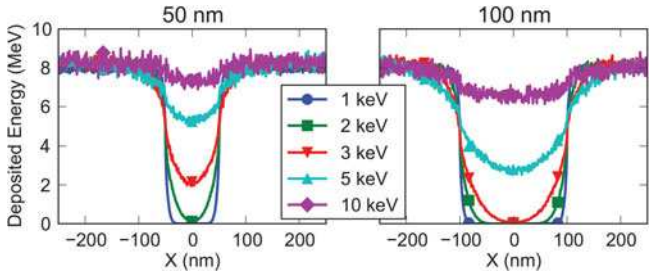

Figure 4. Simulation of the deposited energy for line scans across a TD, located at 0 nm, in GaN with a cylinder radius (modeling the diffusion length near TD) of 50 and 100 nm. The incident energy was varied from 1 to 10 keV. The number of electrons N_0 was changed to keep the nominal deposited energy constant ($E_0 \times N_0$ = 10,000 keV).

backscattered electrons escaping the sample. At higher energy, energy deposition can occur in the SiC substrate and does not contribute to the GaN CL signal. The minimum CL emission occurs at the TD center. A signal greater than zero, at this position, means that the interaction volume is larger than the diffusion length (modeled by the cylinder radius) and energy deposition occurred in the GaN layer (CL emission). To analyze the effect of incident energy on the CL emission, we have calculated the signal-to-noise-ratio (SNR) for each deposited energy line scan across a 50- and 100-nm cylinder radius (diffusion length). The calculated SNR are reported in Table 1. Following the definition of Rose (1948), the SNR is calculated as

$$\mathrm{SNR} = \frac{\Delta E}{std(E_{\mathrm{DFA}})} = \frac{E_{\mathrm{DFA}} - E_{\mathrm{TD}}}{std(E_{\mathrm{DFA}})}, \qquad (2)$$

where E_{DFA} is the energy deposited in a dislocation free area (DFA) and E_{TD} is the energy deposited at the center of

Table 1. Analysis of the Amount of Deposited Energy from Line Scans over a Cylinder Radius of 50 and 100 nm.*

Energy (keV)	SNR	
	50 nm	100 nm
1	90	90
2	90	92
3	72	92
5	40	66
10	22	28

*The cylinder was used to model a threading dislocation (perpendicular to the sample surface) and charge diffusion in a GaN substrate of 2 μm thickness. The SNR was calculated for different incident electron energies.

the TD. The noise contribution $std(E_{DFA})$ is calculated from the standard deviation of the energy deposited in a DFA. A better SNR is obtained at low energy. At 2 keV, the interaction volume is larger than the smaller cylinder radius, which explains why the signal did not reach zero in the middle of the TD. The difference observed in the CL contrast between two cylinder radii in Figure 4 shows the link between the interaction volume and the diffusion length. This relationship is shown in Figure 5, where line scans with cylinder radius between 50 and 125 nm were simulated. The signal at the TD decreases toward zero with an increase of the cylinder radius (defined by the diffusion length). At 3 keV, the Kanaya-Okayama range (Kanaya & Okayama, 1972) is approximately 153 nm in GaN. This value is similar to the diffusion length (125 nm), where the signal gets close to zero. At 5 keV, the Kanaya-Okayama range is around 360 nm and is much larger than the simulated cylinder radius. This larger interaction volume explains the smaller difference in signal between the TD center and the dislocation free area observed at 5 keV in Figure 5.

This MC modeling analysis demonstrates that low energy CL analysis of TDs in GaN provides a better SNR than high energy CL. The smaller interaction volume (25 nm at 1 keV) at lower energy allows nanometer-scale spatial resolution of CL imaging.

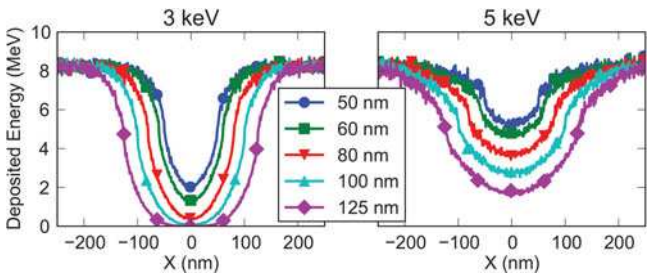

Figure 5. Simulation of the deposited energy for line scans across a TD, located at 0 nm, in GaN with incident energy of 3 and 5 keV. The cylinder radius (modeling the diffusion length near TD) was varied from 50 to 125 nm. The number of electrons N_0 was changed to keep the nominal deposited energy constant ($E_0 \times N_0 = 10{,}000$ keV).

Modeling Energy Deposition in Electron-Beam Resist

In the second application, CASINO has been used to model the total energy deposition spatial distribution to study the effect of incident energy on EBL. Electron-beam lithography is a widely used tool for the manufacture of semiconductor devices either through photomask fabrication or by a direct writing process. In both cases, proximity correction is crucial for effective high-density patterning. This technique allows better correlation between the pattern written on the photomask or substrate and the pattern design. Correction of the pattern for proximity effects during electron-beam writing requires knowledge of the spatial distribution of the deposited energy.

Standard EBL uses a single scanned electron beam to write the pattern on the resist. The writing of a complete chip pattern will take hours. The multibeam scheme decreases the writing time by using multiple parallel electron beams (Pease & Chou, 2008). Current multielectron-beam schemes use incident electron energies ranging from 5 to 100 keV (Liu & Prescop, 2011). Using CASINO to model the total energy deposition spatial distribution, two incident electron energies, 5 and 100 keV, are compared in this section.

Figure 6 shows the spatial distribution of deposited energy in PMMA film for one electron beam. Figure 6A shows a side or cross-section view (XZ) schematic of the sample, electron-beam position, and analyzed volume. A cylindrical distribution was used to calculate the spatial distribution over a radius of 60 μm around the beam position and a depth of 100 nm; the step size was 2 nm for both directions. An electron-beam diameter of 2 nm was used for both energies. Ten million electron trajectories were simulated to decrease the statistical variation inherent of the MC method. In Figure 6B, the radial profile was calculated by summing the deposited energy in the 100-nm-thick PMMA film. The deposited energy at 5 keV was more than one order of magnitude higher than at 100 keV for the same area and electron dose (number of electrons). However, no energy deposition was observed after a radial distance of 560 nm. At 100 keV, the backscattered electrons from the Si substrate can deposit energy in the resist up to 59 μm from the beam position. The contribution of backscattered electrons to the deposit energy distribution was not separated from the contribution of other electrons. However, the 3D display in CASINO was used to visualize the electron trajectories with different color for primary electrons (forward scattering) and backscattered electrons (backward scattering) (Demers et al., 2011). Accurate proximity effect corrections are needed for energy of 100 keV.

In Figure 6C and 6D the depth-radial (ZR) distributions of the deposited energy was compared around the electron-beam position. The color bar used ranges from black, red, yellow to white as the deposited energy density increases. A larger deposited energy profile was observed at 5 keV. Resist regions, where the deposited energy level

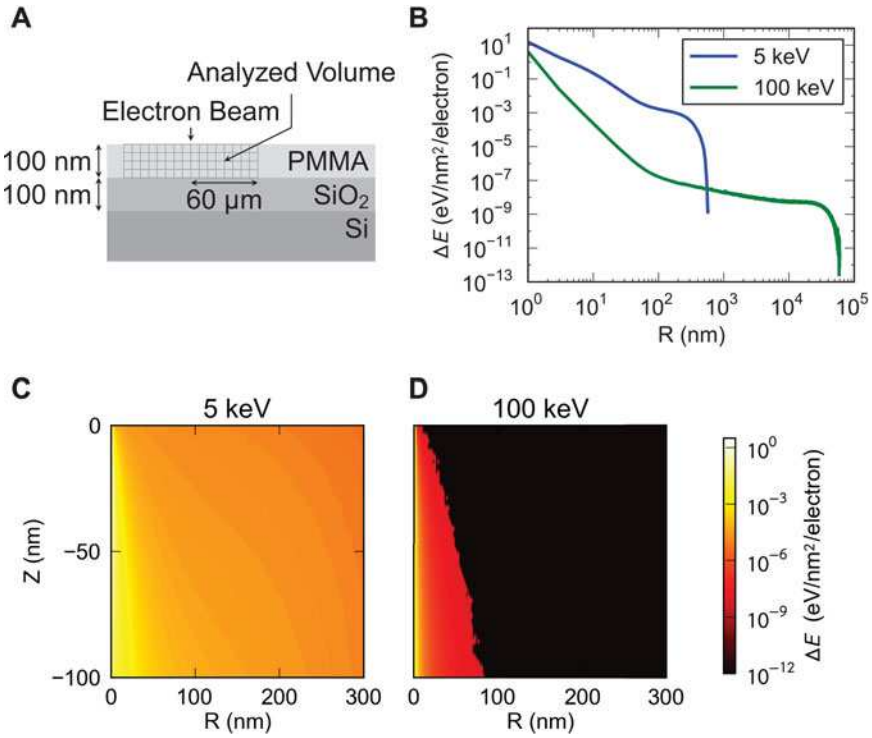

Figure 6. Simulated spatial distribution of the deposited energy ΔE in a 100-nm-thick PMMA film with incident energy of 5 and 100 keV. **A:** Schematic of the sample geometry (not to scale) used for the simulation. The analyzed volume is also shown. **B:** Radial distribution of the total deposited energy (summed over the film thickness). **C**, **D:** Depth-radial (ZR) distribution of the deposited energy for incident energy of 5 and 100 keV, respectively. The deposited energy was color coded on a logarithmic scale.

reaches the resist threshold dose, are exposed and define the spatial resolution of the pattern. For electron-beam writer using energy of 5 keV, a different resist approach is needed to ensure a sub-20-nm spatial resolution. One approach required the use of thinner resist, which may require a second layer to ensure pattern transferability into substrate (Icard et al., 2009). Another approach is to use a resist with a higher threshold dose to compensate for the large spatial resolution. However, a more complex proximity correction is needed for a 100-keV electron-beam writer because of the μm scale range of the backscattered electron. Proximity effect correction programs can use these simulated distributions as input parameter (point spread function). Also the choice of resist used in the simulation in CASINO is not limited to PMMA. The program only needs to know the composition and the mass density of the resist. Chemically amplified resist or hydrogen silsesquioxane resist could have been used instead of PMMA in the simulation.

The energy deposited dose in resist with 3D topography features was adjusted to obtain a uniform exposure of the resist not only laterally but also as a function of the depth using CASINO. Resists with topographic features are used to create 3D structures for various applications in optics, fluidics, or biosciences. One method to obtain these 3D structures is the combination of nanoimprint lithography (NIL) and EBL (Schleunitz et al., 2011). Figure 7A shows a schematic of the process sequence. First, a thermal NIL process is used to imprint a repeated 250 $\times$ 250 nm^2 topography pattern in a 1-μm-thick PMMA film. Subsequently, a grayscale EBL is used to define a line pattern over the relief pattern. In grayscale EBL, the incident electron dose is adjusted to only expose the resist up to a specific depth, i.e., the resist film is not completely exposed. Figure 7B shows the effect of the topographic structure on the lateral-depth (XZ) distribution of the deposited energy for a uniform electron dose, a line pattern, 2-nm step size, and an electron-beam diameter of 2 nm. The color bar used ranges from black, red, yellow to white as the deposited energy density increases. The simulation was obtained with incident electron energy of 100 keV and dose of 3,800 μC/cm^2. The electron-beam shot noise effect is simulated using a Poisson distribution of the nominal number of electrons for each scan point. The 3D structure results in a nonuniformly deposited energy in the lateral direction at a specific depth as seen in Figure 7D. The profile was obtained by summing the deposited energy in a 160-nm-thick layer at the depth of 750 nm (from the top surface). The profile was used to correct the electron dose of the line pattern by increasing the incident dose (8,200 μC/cm^2) when the electron-beam is above the thicker section of the PMMA film. Figure 7C shows the corrected lateral-depth (XZ) distribution, and Figure 7E confirms the uniform dose profile at the depth of 750 nm. The deposited energy was not uniform for all depths as observed on the XZ distribution, but uniform only for the specified depth. However, similar corrections can be obtained for different specific depths. This dose correction with CASINO allows a uniform lateral grayscale EBL on a 3D feature resist.

The proximity effect for a dense line pattern was simulated with CASINO. Figure 8A shows a top view (XY) schematic of the sample, lithography line patterns, and analyzed volume. The lithography pattern consisted of a 5 $\times$ 5 μm^2 area with 110 parallel lines of dimension 26 nm $\times$ 5 μm. The separation between lines is set to 25 nm and the electron-beam scanning step size is 2 nm. The total number of scan points for this 110 lines pattern was 3.6 mil-

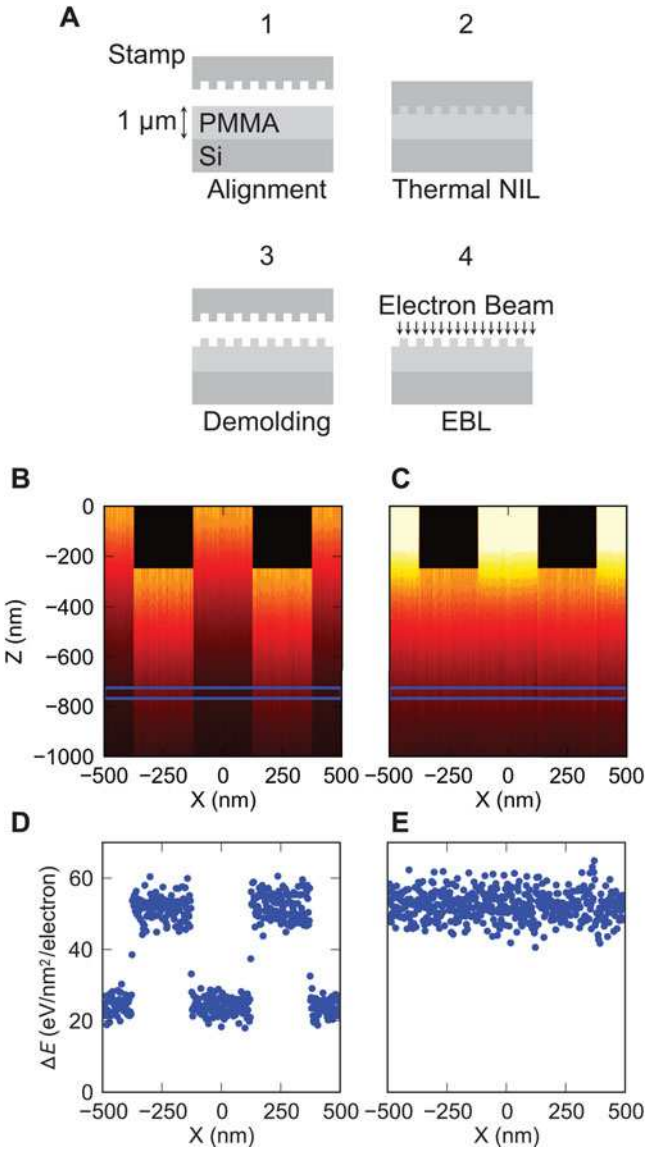

Figure 7. Simulation of the proximity effect correction, for the generation of a mixed 3D pattern combining thermal nanoimprint lithography (NIL) and electron-beam lithography (EBL). **A:** Schematic of the process sequence: NIL and EBL (adapted from Fig. 1 in Schleunitz et al., 2011). **B:** Deposited energy side view (*XZ*) without electron dose correction. **C:** Deposited energy side view (*XZ*) with electron dose correction. The deposited energy was color coded on a logarithmic scale. **D**, **E:** Deposited energy profile obtained from the blue rectangle region in images **B** and **C**, respectively.

lion ($3.575 \cdot 10^6$). In this work, we neglect the effect of simultaneously multibeam exposure, where interaction between the beams and electrons inside the resist could affect the deposited energy by Coulomb interactions (Han et al., 1998). The electron-beam shot noise effect was simulated using a Poisson distribution of the nominal number of electrons for each scan point. Only a partial volume of the exposed area is included in the 3D energy deposition matrix. However, the scan points outside the analyzed volume are still contributing to the deposited energy in this volume

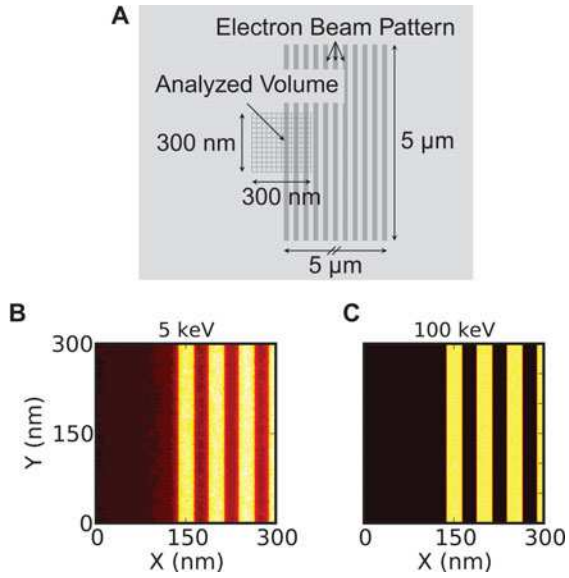

Figure 8. Monte Carlo simulation of the total deposited energy, top view (*XY*), in PMMA generated from EBL line patterns. **A:** Schematic of the sample geometry (not to scale) used for the simulation. The line patterns and the analyzed volume are also shown. **B**, **C:** Deposited energy images for an incident energy of 5 and 100 keV, respectively. The electron doses were 275 μC/cm^2 at 5 keV and 3000 μC/cm^2 at 100 keV. The deposited energy was color coded on a logarithmic scale.

because of the electron diffusion. The 3D matrix size of the analyzed volume is $300 \times 300 \times 100$ nm^3 and is positioned on the center of the first line on the left. See Figure 8A for an illustration of the matrix position relative to the sample and the lithography line patterns. The number of divisions in each dimension was chosen to obtain a unit volume of $2 \times 2 \times 2$ nm^3, which is the similar to the PMMA molecule size (Chen & Ahmed, 1997). Figure 9A shows a side or cross-section view (*XZ*) schematic of the sample, including the lithography line patterns, and the analyzed volume.

Figure 8B, 8C, 9B, and 9C depict the total deposited energy in 100 nm of PMMA resist after the electron-beam exposure of 110 lines patterns at 5 and 100 keV on a silicon substrate with a 100-nm-thick silicon dioxide layer. The color bar used ranges from black, red, yellow to white as the deposited energy density increases.

The electron doses were 275 μC/cm^2 at 5 keV and 3,000 μC/cm^2 at 100 keV. These dose values were found by simulation of the 5-keV line pattern with different electron doses until the same total deposited energy in a line pattern for both energies was obtained. The multiple simulations were needed because the small thickness of the resist film did not allow a linear prediction with accelerating voltage.

Modification of the pattern prior to development is performed in regions where the energy level reaches the resist threshold dose outside the desired area. The resist threshold dose is not exactly known for PMMA, but it is on the order of a few eV. A value of 3.3 eV was reported (Aktary et al., 2006) from reactive molecular dynamics simulations (Stoliarov et al., 2003) for the main-chain C-C bonds. For

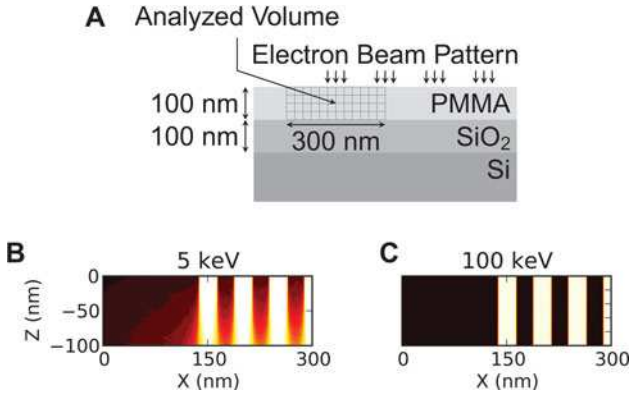

Figure 9. Monte Carlo simulation of the total deposited energy, side view (*XZ*), in PMMA generated from EBL line patterns. **A:** Schematic of the sample geometry (not to scale) used for the simulation. The line patterns and the analyzed volume are also shown. **B**, **C:** Deposited energy images for an incident energy of 5 and 100 keV, respectively. The electron doses were 275 μC/cm^2 at 5 keV and 3,000 μC/cm^2 at 100 keV. The deposited energy was color coded on a logarithmic scale.

our analysis, the exact amount of deposited energy is not important; any location with deposited energy would be developed.

Figures 8B and 8C show a top view (*XY*) of the deposited energy, summed over the 100-nm PMMA layer (*Z*). At 5 keV, energy was deposited between the lines so that the lithography is likely to fail. Also, the lower dose used at 5 keV creates a nonuniform deposited energy distribution in a line pattern as observed in Figure 8B. The variation in the number of electrons for each scan point from the shot noise of the electron gun creates this variation in deposited energy. At 100 keV, no deposited energy was visible between two lines, and the line edges were sharp and will result in a good lithography patterns after development.

Figures 9B and 9C show a side view (*XZ*) of the energy summed over 300 nm in the *YZ*-axis in the PMMA layer. The side view at 5 keV shows that the deposited energy between the lines is more important at the bottom, where the interaction volume becomes larger. From the first line at the left, we observed that energy may be deposited as far as 150 nm (at the bottom) from the line pattern at 5 keV. At 100 keV no deposition was observed outside the line pattern.

The modeling of the deposited energy, such as shown in Figures 8 and 9, can assist in the determination of the exposure parameters and resist thickness. Once the resist exposure parameters such as accelerating voltage and dose are optimized, the nanometer-scale semiconductor devices can be successfully fabricated.

Conclusions

New modules have been added to the MC software CASINO Version 3 that provide the simulation of complex beam scanning patterns and the calculation of the deposited energy by region and inside subregions of a 3D volume. Two examples were presented on the application of the new energy deposition modeling capabilities of CASINO. First, CL emission near threading dislocations in GaN was simulated, and second, the exposure parameters for PMMA resist using EBL were determined.

The CASINO features, 3D sample, total deposited energy per region distribution, and image scan point provide a way to simulate CL emission near threading dislocations in GaN. The modeling showed that using lower incident electron energy provides a better SNR than higher energy even if the high energy gives higher CL signal.

The advantage and disadvantage of two different multibeam EBL schemes were obtained using the 3D volume of the total deposited energy and the complex beam scanning patterns features of CASINO. The simulation showed that a higher threshold resist was needed at 5 keV to compensate for the large spatial spread. However, at 100 keV, a more complex proximity correction was needed because of the long range of the backscattered electrons. A uniform deposition dose for a nonflat resist or complex exposure pattern was obtained by adjusting the nominal electron dose for specific features. Using these simulations the dose can be adjusted to obtain a uniform exposure of the resist not only laterally but also as a function of the depth. The simulation showed that 26-nm-wide line patterns in 100-nm-thick PMMA on SiO_2/Si substrate was not successfully exposed with 5-keV incident electron energy, but was successful at 100 keV. Our calculations emphasize that the simulation of the energy deposition allows the optimization of the exposure parameters, such as accelerating voltage and electron dose. The spatial distribution of the deposited energy can be used as the first step of the complete simulation of the EBL process.

References

Adesida, I., Everhart, T.E. & Shimizu, R. (1979). High resolution electron-beam lithography on thin films. *J Vac Sci Technol* **16**(6), 1743–1748.

Aktary, M., Stepanova, M. & Dew, S.K. (2006). Simulation of the spatial distribution and molecular weight of polymethylmethacrylate fragments in electron beam lithography exposures. *J Vac Sci Technol B* **24**(2), 768–779.

Babin, S., Borisov, S., Ivanchikov, A. & Ruzavin, I. (2006). Modeling of linewidth measurement in SEMs using advanced Monte Carlo software. *J Vac Sci Technol B* **24**(6), 3121–3124.

Barjon, J., Brault, J., Daudin, B., Jalabert, D. & Sieber, B. (2003). Cathodoluminescence study of carrier diffusion in AlGaN. *J Appl Phys* **94**(4), 2755–2757.

Bishop, H.E. (1965). A Monte Carlo calculation on the scattering of electrons in copper. *Proc Phys Soc* **85**(5), 855–866.

Chen, W. & Ahmed, H. (1997). Nanofabrication for electronics. In *Advances in Imaging and Electron Physics*, Hawkes, P.W. (Ed.), pp. 87–185. New York: Academic Press.

de Jonge, N., Poirier-Demers, N., Demers, H., Peckys, D.B. & Drouin, D. (2010). Nanometer-resolution electron microscopy through micrometers-thick water layers. *Ultramicroscopy* **110**(9), 1114–1119.

Demers, H., Poirier-Demers, N., Couture, A.R., Joly, D., Guilmain, M., de Jonge, N. & Drouin, D. (2011). Three-dimensional

electron microscopy simulation with the CASINO Monte Carlo software. *Scanning* **33**(3), 135–146.

Drouin, D., Couture, A.R., Joly, D., Tastet, X., Aimez, V. & Gauvin, R. (2007). CASINO V2.42—A fast and easy-to-use modeling tool for scanning electron microscopy and microanalysis users. *Scanning* **29**(3), 92–101.

Drouin, D., Hovington, P. & Gauvin, R. (1997). CASINO: A new Monte Carlo code in C language for electron beam interaction—Part II: Tabulated values of Mott cross section. *Scanning* **19**(1), 20–28.

Fleischer, K., Toth, M., Phillips, M.R., Zou, J., Li, G. & Chua, S.J. (1999). Depth profiling of GaN by cathodoluminescence microanalysis. *J Appl Phys* **74**(8), 1114–1116.

Gauvin, R. & L'Espérance, G. (1992). A Monte Carlo code to simulate the effect of fast secondary electron on k_{AB} factors and spatial resolution in the TEM. *J Microsc* **168**(2), 153–167.

Gelhausen, O., Phillips, M.R. & Toth, M. (2001). Depth-resolved cathodoluminescence microanalysis of near-edge emission in III-nitride thin films. *J Appl Phys* **89**(6), 3535–3537.

Glezos, N. & Raptis, I. (1996). A fast electron beam lithography simulator based on the Boltzmann transport equation. *IEEE T Comput Aid Design Int Circ Syst* **15**(1), 92–102.

Glezos, N., Raptis, I., Tsoukalas, D. & Hatzakis, M. (1992). Application of a new analytical technique of electron distribution calculations to the profile simulation of a high sensitivity negative electron-beam resist. *J Vac Sci Technol B* **10**(6), 2606–2609.

Greeneich, J.S. & Duzer, T.V. (1974). An exposure model for electron-sensitive resists. *IEEE T Electron Dev* **21**(5), 286–299.

Han, L., McCord, M.A., Winograd, G.I. & Pease, R.F.W. (1998). Performance investigation of Coulomb interaction-limited high throughput electron beam lithography based on empirical modeling. *J Vac Sci Technol B* **16**(6), 3215–3220.

Holt, D.B. & Napchan, E. (1994). Quantification of SEM EBIC and CL signal using Monte Carlo electron-trajectory simulations. *Scanning* **16**(2), 78–86.

Hovington, P., Drouin, D. & Gauvin, R. (1997*a*). CASINO: A new Monte Carlo code in C language for electron beam interaction—Part I: Description of the program. *Scanning* **19**(1), 1–14.

Hovington, P., Drouin, D., Gauvin, R., Joy, D.C. & Evans, N. (1997*b*). CASINO: A new Monte Carlo code in C language for electron beam interaction—Part III: Stopping power at low energies. *Scanning* **19**(1), 29–35.

Icard, B., Rio, D., Veltman, P., Kampherbeek, B., Constancias, C. & Pain, L. (2009). Development of resist process for 5-KV multi-beam technology. In *Proc SPIE 7271*, Schellenberg, F.M. & La Fontaine, B.M. (Eds.), pp. 72710R. San Jose, CA.

Joy, D.C. (1995). *Monte Carlo Modeling for Electron Microscopy and Microanalysis*. New York: Oxford University Press.

Joy, D.C. & Luo, S. (1989). An empirical stopping power relationship for low-energy electrons. *Scanning* **11**(4), 176–180.

Kanaya, K. & Okayama, S. (1972). Penetration and energy-loss theory of electrons in solid targets. *J Phys D Appl Phys* **5**(1), 43–58.

Kim, S.-H., Ham, Y.-M., Lee, W. & Chun, K. (1998). New approach of Monte Carlo simulation for low energy electron beam lithography. *Microelectron Eng* **41–42**, 179–182.

Kyser, D.F. & Viswanathan, N.S. (1975). Monte Carlo simulation of spatially distributed beams in electron-beam lithography. *J Vac Sci Technol* **12**(6), 1305–1308.

Liu, E.D. & Prescop, T. (2011). Optimization of e-beam landing energy for EBDW. In *Proc SPIE 7970*, Herr, D.J.C. (Ed.), pp. 79701S. San Jose, CA.

McCarthy, L., Smorchkova, I., Xing, H., Fini, P., Keller, S., Speck, J., DenBaars, S.P., Rodwell, M.J.W. & Mishra, U.K. (2001). Effect of threading dislocations on AlGaN/GaN heterojunction bipolar transistors. *Appl Phys Lett* **78**(15), 2235–2237.

Murata, K., Kawata, H., Nagami, K., Hirai, Y. & Mano, Y. (1987). Studies of energy dissipation in resist films by a Monte Carlo simulation based on the Mott cross section. *J Vac Sci Technol B* **5**(1), 124–128.

Murata, K., Kyser, D.F. & Ting, C.H. (1981). Monte Carlo simulation of fast secondary electron production in electron beam resists. *J Appl Phys* **52**(7), 4396–4405.

Newbury, D.E. & Myklebust, R.L. (1981). A Monte Carlo electron trajectory simulation for analytical electron microscopy. In *Analytical Electron Microscopy*, Geiss, R.H. (Ed.), pp. 91–98. San Francisco, CA: San Francisco Press.

Nouiri, A. & Aouati, R. (2008). Monte Carlo model of cathodoluminescence characterization of AlAs/GaAs/AlAs laser diode. *Physica E* **40**(5), 1751–1753.

Pauc, N., Phillips, M.R., Aimez, V. & Drouin, D. (2006). Carrier recombination near threading dislocations in GaN epilayers by low voltage cathodoluminescence. *Appl Phys Lett* **89**(16), 161905.

Pease, R.F. & Chou, S.Y. (2008). Lithography and other patterning techniques for future electronics. *Proc IEEE* **96**(2), 248–270.

Raptis, I., Glezos, N. & Hatzakis, M. (1993). Analytical evaluation of the energy deposition function in electron-beam lithography in the case of a composite substrate. *Proc 16th Int Symp Electron Ion* **11**(6), 2754–2757.

Reimer, L. (1998). *Scanning Electron Microscopy: Physics of Image Formation and Microanalysis*. Berlin: Springer.

Rose, A. (1948). Television pickup tubes and the problem of vision. In *Advances in Electronics and Electron Physics*, Marton, L. (Ed.), pp. 131–166. New York: Academic Press.

Schleunitz, A., Spreu, C., Vogler, M., Atasoy, H. & Schift, H. (2011). Combining nanoimprint lithography and a molecular weight selective thermal reflow for the generation of mixed 3D structures. *J Vac Sci Technol B* **29**(6), 06FC01.

Stepanova, M., Fito, T., Szabó, Z., Alti, K., Adeyenuwo, A.P., Koshelev, K., Aktary, M. & Dew, S.K. (2010). Simulation of electron beam lithography of nanostructures. *J Vac Sci Technol B* **28**(6), C6C48–C46C57.

Stoliarov, S.I., Westmoreland, P.R., Nyden, M.R. & Forney, G.P. (2003). A reactive molecular dynamics model of thermal decomposition in polymers: I. Poly(methyl methacrylate). *Polymer* **44**(3), 883–894.

Toth, M. (2006). Microcharacterization of GaN defect structure. PhD Thesis. Sydney, Australia: University of Technology.

Toth, M. & Phillips, M.R. (1998). Monte Carlo modeling of cathodoluminescence generation using electron energy loss curves. *Scanning* **20**(6), 425–432.

Zhou, J. & Yang, X. (2006). Monte Carlo simulation of process parameters in electron beam lithography for thick resist patterning. *J Vac Sci Technol B* **24**(3), 1202–1209.